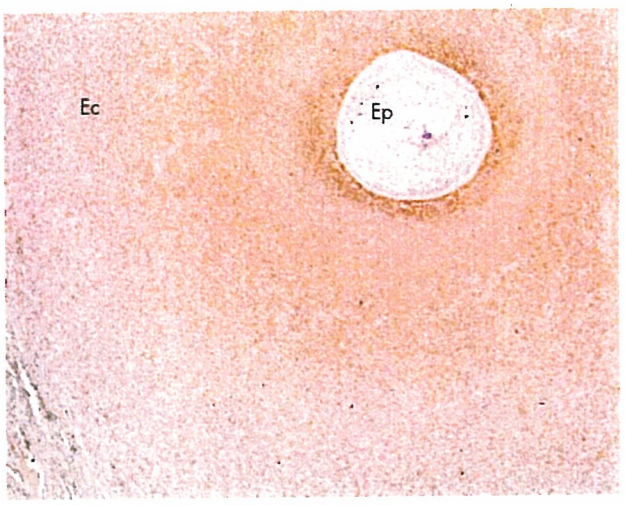

Figure 3 Ameloblastic fibroma, consisting of odontogenic epithelial follicle (Ep) and ectomesenchymal tissue (Ec). Nestin was expressed in the odontogenic ectomesenchymal cells, particularly around the epithelial component.

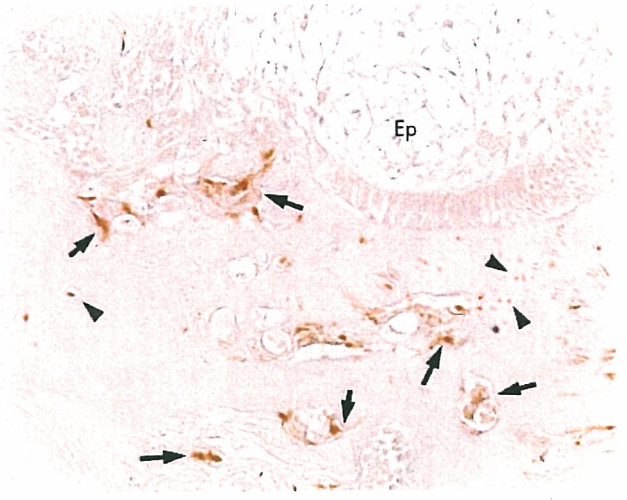

Figure 4 Dentinoid matrix included in the ameloblastic fibrodentinoma. The odontogenic epithelial component (Ep) is adjacent to the dentinoid. Intense reactivity with nestin was found in the plump cells adhering to the dentinoid (arrows) and dentinal fibres (arrow heads).

odontogenic epithelial islands within the tumour, but the other eight cases contained no odontogenic epithelial elements.

DISCUSSION

It seems reasonable that some odontogenic tumours express nestin because odontogenic ectomesenchymal tissue is derived from neural crest.[18–20] However, nestin associated with human odontogenic ectomesenchyme is not expressed throughout life, but rather during limited periods such as odontogenesis and repair of dentine.[13 15 21] In addition, our characterisation of odontogenic ectomesenchymal tissues indicated no differentiation towards muscle and nervous tissues, and immunohistochemical examination revealed intriguing localisation and distribution of nestin in various odontogenic tumours.[17]

Ameloblastomas and malignant ameloblastomas, which contain no odontogenic ectomesenchyme, did not express nestin, except for one benign case that showed focal nestin localisation in the apical part of the peripheral columnar epithelium of the follicular pattern. In contrast, odontogenic mixed tumours such as ameloblastic fibroma, ameloblastic fibro-odontoma, ameloblastic fibrodentinoma, and ameloblastic fibrosarcoma demonstrated intense expression in the odontogenic ectomesenchymal element, particularly around the neoplastic follicular odontogenic epithelium. In addition, some follicular epithelial components showed nestin localisation in both peripheral ameloblastic columnar cells and inner stellate cells. We also found similar findings in the odontogenic fibroma containing non-neoplastic odontogenic epithelial strands. In human odontogenic tumours, nestin is thought to be expressed in association with mutual interaction between odontogenic epithelium and ectomesenchyme. This is strongly supported by our histological finding that the ectomesenchymal cells around the follicular odontogenic epithelium showed intense reaction and weak or no reactivity further away from the epithelium.

The histogenesis of jaw myxoma is still controversial. Two origins of spindle or stellate tumour cells intermingled within the mucoid matrix have been proposed—that is, dental papilla cells of tooth germ,[22 23] and mesenchymal cells such as fibroblasts or myofibroblasts other than odontogenic ectomesenchyme.[24–26] In our study, almost half the cases of jaw myxoma demonstrated nestin immunoexpression. From the viewpoint of specific nestin immunoreactivity in odontogenic ectomesenchyme, this result implies that there are those two possible histogeneses of myxoma affecting the jaw. Absence of odontogenic epithelium does not always implicate non-odontogenic origin, as three myxomas without odontogenic epithelium were positive for nestin.

In the odontomas, nestin expression was observed in mature odontoblasts and their processes in the dentinal tubules. The gradient of nestin staining in pulp cells followed differentiation toward the odontoblasts. The same findings were observed in the odontoma-like tissues in the ameloblastic fibro-odontomas. The nestin expression in these lesions may be related to acquisition of the dentine producing function. The phenomenon occurring in odontoma is similar to that in the pulp–odontoblast complex in cases of human dental caries and repair after tooth injury;[15 21] the dentine matrix is produced in these conditions. Moreover, in the ameloblastic fibrodentinomas, flat or plump cells attached to the dentinoid matrix and their processes in the irregular dental tubules were positive for nestin. Although these cells are morphologically different from the mature odontoblasts, the findings suggest that they participate in producing the dentinoid matrix. The rate of nestin positive cases of odontoma was somewhat lower than in other tumours. We consider that nestin expression is under the influence of the differential stages for differentiation. Its expression is lacking in the human completed permanent tooth, as opposed to the tooth germ and developing tooth. The reason for the low positive rate may be that odontoma is composed of differentiated dental components. In fact, some cases, including differentiated odontoblasts and pulp cells mimicking these of intact permanent tooth, did not express nestin. 5

AOT is not believed to be a true neoplasm, but has varying degrees of inductive change in the connective tissue.[17] Our interesting result for AOT was that nestin was distributed predominantly in the epithelial component. Intense nodular reaction took place in the focal whorled masses of spindle cells and rosette-like structures indicating rows of radial columnar cells, where eosinophilic droplets were found by haematoxylin and eosin staining to be present in the epithelium. AOT is morphologically composed of some types of epithelium. The columnar or spindle epithelium associated with hyaline droplets has a different immunophenotype from other cells.[27–29] Tatemoto *et al*,[30] who investigated localisation of cytoplasmic skeletal filaments in AOT, emphasised that

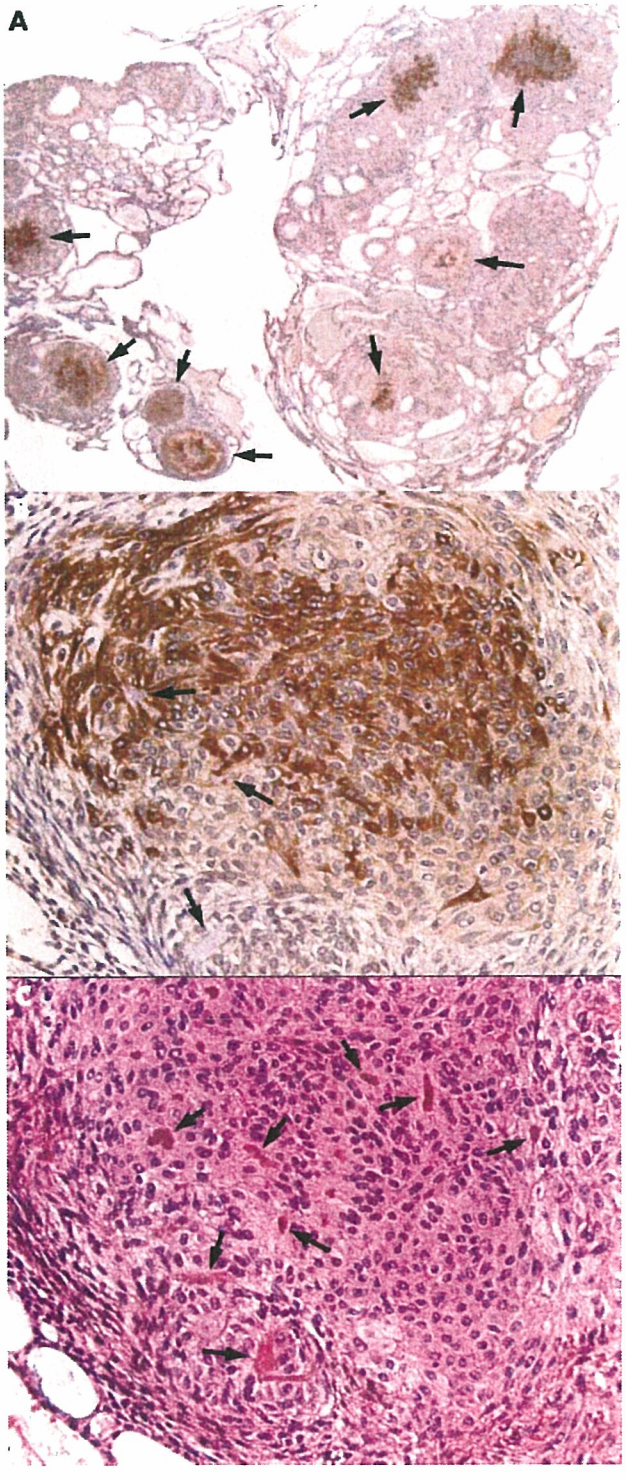

Figure 5 (A) AOT displayed intense nestin expression in the scattered nodular foci (arrowheads) and rosette arrangements (arrows) of neoplastic tumour cells. (B) Whorled spindle cells in AOT showed strong nestin immunoreactivity. Basophilic amorphous deposits were observed in the tumour cells (arrows). (C) Serial section of (B) stained with haematoxylin and eosin; hyaline droplets were scattered within the tumour (arrows).

spindle or columnar epithelium showed very slight reaction with all antibodies to keratins, whereas small and compact cells at the periphery of the focus of spindle or columnar epithelium indicated slight to moderate expression of keratin and vimentin, and showed coexpression. These investigations

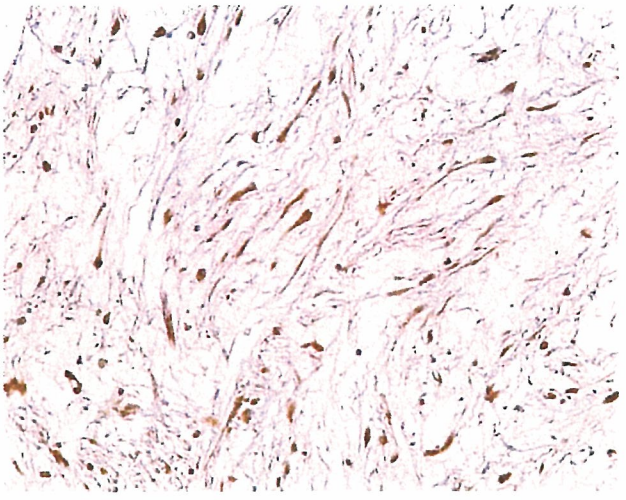

Figure 6 Spindle or reticular tumour cells in the myxoma demonstrated nestin immunoexpression.

suggest that the epithelial cells composing AOT are not homogenous. Our study also indicated a heterogeneous pattern of nestin localisation in the AOT. Nestin is supposed to be expressed in association with the production of eosinophilic deposit in the tumour.

The rate of nestin positive cases is variable among odontogenic tumours and jaw myxoma. This may be a result of different origin, such as myxoma, and different stages for differentiation. In addition, it is possibly that the decalcification procedure used may destoy the molecular structure of the antigen. However, we consider that nestin can be regarded as a marker for odontoblasts and odontogenic ectomesenchymal cells in odontogenic tumours.

The supplemental figures can be viewed on the JCP website at http://www.jclinpath.com/supplemental.

TAKE HOME MESSAGES

- Nestin, a cytoskeleton intermediate filament, is a marker of neural stem cells or progenitor cells, and its expression is also related to tooth development and repair of dentine.
- Nestin expression was immunohistochemically examined using several antibodies on 138 tumours.
- Almost all the ameloblastomas and malignant ameloblastomas were negative for nestin, whereas odontogenic ectomesenchyme in the odontogenic mixed tumours expressed nestin. Nestin was found in neoplastic cells in almost half cases of jaw myxoma and one case of odontogenic fibroma.
- The distribution of nestin in the odontogenic mixed tumours suggests that its expression is upregulated by stimulation from odontogenic epithelium. It may also be involved in the differentiation from pulp cells to odontoblasts in odontogenic tumours.
- Nestin is a useful marker for the odontogenic ectomesenchyme and odontoblasts in odontogenic tumours.

Authors' affiliations

S Fujita, T Ikeda, Division of Oral Pathology and Bone Metabolism, Department of Developmental and Reconstructive Medicine, Nagasaki University Graduate School of Biomedical Sciences, Nagasaki, Japan
K Hideshima, Division of Oral and Maxillofacial Surgical Reconstruction and Functional Restoration, Department of Developmental and Reconstructive Medicine, Nagasaki University Graduate School of Biomedical Sciences, Nagasaki, Japan

REFERENCES

1 **Lendahl U**, Zimmerman LB, McKay RD. CNS stem cells express a new class of intermediate filament protein. *Cell* 1990;**60**:585–95.
2 **Kachinsky AM**, Dominov JA, Miller JB. Myogenesis and the intermediate filament protein, nestin. *Dev Biol* 1994;**165**:216–28.
3 **Sejersen T**, Lendahl U. Transient expression of the intermediate filament nestin during skeletal muscle development. *J Cell Sci* 1993;**106**:1291–300.
4 **Kachinsky AM**, Dominov JA, Miller JB. Intermediate filaments in cardiac myogenesis: nestin in the developing mouse heart. *J Histochem Cytochem* 1995;**43**:843–7.
5 **Frojdman K**, Pelliniemi LJ, Lendahl U, *et al.* The intermediate filament protein nestin occurs transiently in differentiating testis of rat and mouse. *Differentiation* 1997;**61**:243–9.
6 **Abdel-Rahman A**, Rao MS, Shetty AK. Nestin expression in hippocampal astrocytes after injury depends on the age of the hippocampus. *Glia* 2004;**47**:299–313.
7 **Frisen J**, Johansson CB, Torok C, *et al.* Rapid, widespread, and longlasting induction of nestin contributes to the generation of glial scar tissue after CNS injury. *J Cell Biol* 1995;**131**:453–64.
8 **Holmin S**, Almqvist P, Lendahl U, *et al.* Adult nestin-expressing subependymal cells differentiate to astrocytes in response to brain injury. *Eur J Neurosci* 1997;**9**:65–75.
9 **Lin RC**, Matesic DF, Marvin M, *et al.* Re-expression of the intermediate filament nestin in reactive astrocytes. *Neurobiol Dis* 1995;**2**:79–85.
10 **Dahlstrand J**, Collins VP, Lendahl U. Expression of the class VI intermediate filament nestin in human central nervous system tumors. *Cancer Res* 1992;**52**:5334–41.
11 **Florenes VA**, Holm R, Myklebost O, *et al.* Expression of the neuroectodermal intermediate filament nestin in human melanomas. *Cancer Res* 1994;**54**:354–6.
12 **Tohyama T**, Lee VM, Rorke LB, *et al.* Nestin expression in embryonic human neuroepithelium and in human neuroepithelial tumor cells. *Lab Invest* 1992;**66**:303–13.
13 **About I**, Laurent-Maquin D, Lendahl U, *et al.* Nestin expression in embryonic and adult human teeth under normal and pathological conditions. *Am J Pathol* 2000;**157**:287–95.
14 **Terling C**, Rass A, Mitsiadis TA, *et al.* Expression of the intermediate filament nestin during rodent tooth development. *Int J Dev Biol* 1995;**39**:947–56.
15 **About I**, Mitsiadis TA. Molecular aspects of tooth pathogenesis and repair: in vivo and in vitro models. *Adv Dent Res* 2001;**15**:59–62.
16 **McLachlan JL**, Smith AJ, Cooper PR. Piezo-power microdissection of mature human dental tissue. *Arch Oral Biol* 2003;**48**:731–6.
17 **Kramer IRH**, Pindborg JJ, Shear M. In:, *World Health Organization, international histological classification of tumours. Histological typing of odontogenic tumours*, 2nd ed. Berlin: Springer-Verlag, 1992:11–27.
18 **Sharpe PT**. Neural crest and tooth morphogenesis. *Adv Dent Res* 2001;**15**:4–7.
19 **Ruch JV**, Lesot H, Begue-Kirn C. Odontoblast differentiation. *Int J Dev Biol* 1995;**39**:51–68.
20 **Slavkin HC**, MacDougall M, Zeichner-David M, *et al.* Molecular determinants of cranial crest-derived odontogenic ectomesenchyme during dentinogenesis. *Am J Med Genet* 1988;**4**(suppl):7–22.
21 **McLachlan JL**, Smith AJ, Sloan AJ, *et al.* Gene expression analysis in cells of the dentine-pulp complex in healthy and carious teeth. *Arch Oral Biol* 2003;**48**:273–83.
22 **Zhao M**, Lu Y, Takata T, *et al.* Immunohistochemical and histochemical characterization of the mucosubstances of odontogenic myxoma: histogenesis and differential diagnosis. *Pathol Res Pract* 1999;**195**:391–7.
23 **Thoma KH**. Tumors of the condyle and temporomandibular joint. *Oral Surg Oral Med Oral Pathol* 1954;**7**:1091–107.
24 **Slootweg PJ**, Wittkampf AR. Myxoma of the jaws. An analysis of 15 cases. *J Maxillofac Surg* 1986;**14**:46–52.
25 **Lombardi T**, Samson J, Bernard JP, *et al.* Comparative immunohistochemical analysis between jaw myxoma and mesenchymal cells of tooth germ. *Pathol Res Pract* 1992;**188**:141–4.
26 **Hasleton PS**, Simpson W, Craig RD. Myxoma of the mandible—a fibroblastic tumor. *Oral Surg Oral Med Oral Pathol* 1978;**46**:396–406.
27 **Takahashi H**, Fujita S, Shibata Y, *et al.* Adenomatoid odontogenic tumour: immunohistochemical demonstration of transferrin, ferritin and alpha-one-antitrypsin. *J Oral Pathol Med* 2001;**30**:237–44.
28 **Murata M**, Cheng J, Horino K, *et al.* Enamel proteins and extracellular matrix molecules are co-localized in the pseudocystic stromal space of adenomatoid odontogenic tumor. *J Oral Pathol Med* 2000;**29**:483–90.
29 **Takata T**, Zhao M, Uchida T, *et al.* Immunohistochemical demonstration of an enamel sheath protein, sheathlin, in odontogenic tumors. *Virchows Arch* 2000;**436**:324–9.
30 **Tatemoto Y**, Tanaka T, Okada Y, *et al.* Adenomatoid odontogenic tumour: co-expression of keratin and vimentin. *Virchows Arch A Pathol Anat Histopathol* 1988;**413**:341–7.

Authors Queries
Journal: **Journal of Clinical Pathology**
Paper: **cp25403**
Title: **Nestin expression in odontoblasts and odontogenic ectomesenchymal tissue of odontogenic tumours**

Dear Author
During the preparation of your manuscript for publication, the questions listed below have arisen. Please attend to these matters and return this form with your proof. Many thanks for your assistance

Query Reference	Query	Remarks
1	GFAP seems to be "fibrillary" rather than "fibrillar" – I only found about 250 references to the latter as opposed to over 250,000 for the former, so I have changed it; is this OK?	
2	JCP uses UK English, so some spellings have been changed	
3	Because of the list style used originally, it appeared that the paragraph after 'Malignant' referred only to those bullet points, whereas it seems it should be both, therefore I have put the bullet points in a table to make this clear; is this OK?	
4	Please give original magnifications	
5	What are 'these' here – differentiated odontoblasts?	

Key Engineering Materials Vols. 309-311 (2006) pp. 1059-1062
online at http://www.scientific.net

Porous Granules of β-Tricalcium Phosphate Composed of Rod-shaped Particles

Koji Ioku[1, a], Giichiro Kawachi[1], Kazuhiko Nakahara[1], Emile Hideki Ishida[1], Hideyuki Minagi[2], Takatoshi Okuda[3,4], Ikuho Yonezasaw[3], Hisashi Kurosawa[3], Tohru Ikeda[4]

[1]Graduate School of Environmental Studies, Tohoku University
Aoba 6-6-20, Aramaki, Aoba-ku, Sendai 980-8579, Japan
[a]ioku@mail.kankyo.tohoku.ac.jp
[2]Technical Research Laboratory, Toyo Kohan Co., Ltd., Kudamatsu, Yamaguchi 744-8611, Japan
[3]Department of Orthopedic Surgery, School of Medicine, Juntendo University, 2-1-1 Hongo, Bunkyo-Ku, Tokyo 113-8421, Japan
[4]Division of Oral Pathology and Bone Metabolism, Department of Developmental and Reconstructive Medicine, Nagasaki University Graduate School of Biomedical Sciences, 1-7-1 Sakamoto, Nagasaki 852-8588, Japan

Keywords: β-TCP, Calcium phosphate, Granule, Porous material, Rod-shape

Abstract. Porous granules of β-tricalcium phosphate (β-$Ca_3(PO_4)_2$; β-TCP) were prepared from porous hydroxyapatite granules with calcium deficient composition synthesized by hydrothermal method. The β-TCP granules were composed of rod-shaped particles of about 10-20 μm in length. Rod-shaped particles were locked together to make micro-pores, and the size of micro-pores formed by tangling of rod-shaped particles was about 0.1-0.5 μm. The granule size, particle size, and micro-pore size could be controlled by our unique method. The porous granules of β-TCP must be suitable for the bone graft material and for scaffold of cultured bone.

Introduction

The difference in microstructure has a large effect on the reaction of bioceramics in the bone. Porous materials of β-TCP have been known to be biocompatible and osteoconductive. Several previous studies have also confirmed that β-TCP is more biodegradable as the implant material than HA [1-3]. In addition, the authors reported that micro-pores of β-TCP with about 0.1-0.5 μm in size were significantly important for bio-resorption in bones [4], therefore micro-pores, as well as macro-pores, must be controlled for porous material design, although the size of micro-pores is too small for cells. The present paper deals with the preparation of porous β-TCP granules with designed microstructure, especially in micro-pores.

Experimental Method

Preparation of materials. Commercial powders of α-tricalcium phosphate (α-$Ca_3(PO)_4$: α-TCP, Taihei Chemical Ind. Co., Ltd., Japan) and gelatin (Wako Pure Chemical Ind., Ltd., Japan) were used as the starting material. The aqueous slurry of α-tricalcium phosphate (α-TCP) with gelatin was prepared. The slurry of α-TCP / gelatin was dropped into stirring vegetable oil at 80 °C, and then the oil was cooling down at 4 °C with keeping stirring. These granules were washed with ethanol, and then they were filtered and dried in air. To remove gelatin and to keep the crystal phase of α-TCP, they were heated at 1200 °C for 5 min, and then set in a 105 cm^3 autoclave with 10 cm^3 of water. The samples were exposed to vapor of water at the temperature from 40 to 160 °C under saturated vapor pressure for 10 h, and then the samples were heated at 900 °C for 3 h in air for preparation of β-TCP.

Characterization of materials. The produced phases were identified by powder X-ray diffractometry with graphite-monochromatized CuKα radiation, operating at 40 kV and 20 mA (XRD; Mac Science, MXP^3, Japan). The samples were dissolved in nitric acid of 0.1 mol·dm^{-3}, and then the chemical composition of them was analyzed by inductively coupled plasma spectrometer (ICP-MS; Seiko Instruments, SPQ 9000, Japan). The microstructure of specimens was observed by scanning electron microscope (SEM; JEOL, JSM-T300, Japan). Pore volume and distribution of pore diameter were measured by mercury intrusion porosimetry (MIP; Carlo Elba, Porosimeter 2000, Italy). Specific surface area was measured by using BET method.

Results and Dissociation

The size of spherical particles of α-TCP with gelatin was depended on the stirring rate of vegetable oil and the viscosity of slurry. After heating at 1200 °C in air, porous spherical α-TCP granules were obtained. After hydrothermal treatment, α-TCP was changed into HA composed of rod-shaped crystals [5].

HA was formed at the temperatures above 40 °C, and then no phases other than HA were revealed by XRD for the samples treated at the temperatures above 105 °C. The produced HA was not stoichiometric HA, that was calcium deficient HA. In general, chemical formula of calcium deficient HA is described as follows: $Ca_{10-x}(HPO_4)_x(PO_4)_{6-x}(OH)_{2-x}\cdot nH_2O$. The authors reported that composition of this apatite could be controlled [6]. The Ca/P ratio of the samples increased from 1.50 to 1.63 with increasing treatment temperature, but the Ca/P ratio of the samples was lower than that of stoichiometric HA (stoichiometric Ca/P=1.67).

Porous HA granules prepared at the temperatures below 80 °C were composed of irregular shaped HA particles. In the contrast, the homogeneous porous structure was observed for the samples treated at the temperatures above 105 °C. Porous HA granules prepared by hydrothermal treatment at 105 °C were composed of rod-shaped crystals elongated along the *c*-axis [7]. The HA crystals were about 5 μm in length at 105 °C, about 10 μm at 120 °C and about 10-20 μm at 160 °C. Rod-shaped crystals were locked together to make micro-pores. The diameter of micro-pore was 0.1-0.5 μm in size. The porosity and the size of micro-pore increased slightly with increasing temperature of the hydrothermal treatment.

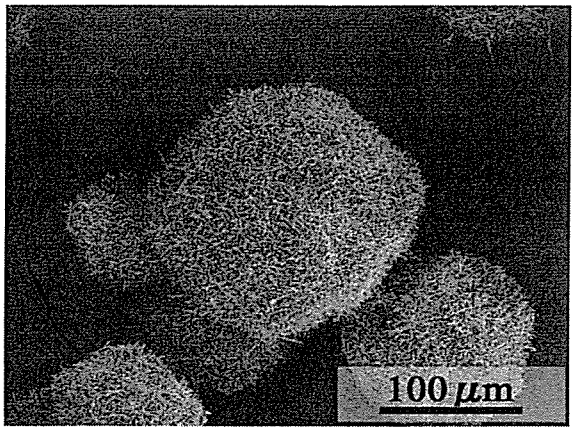

Fig.1 SEM image of β-TCP granules obtained by sintering at 900 °C from HA granules prepared by hydrothermal treatment at 160 °C.

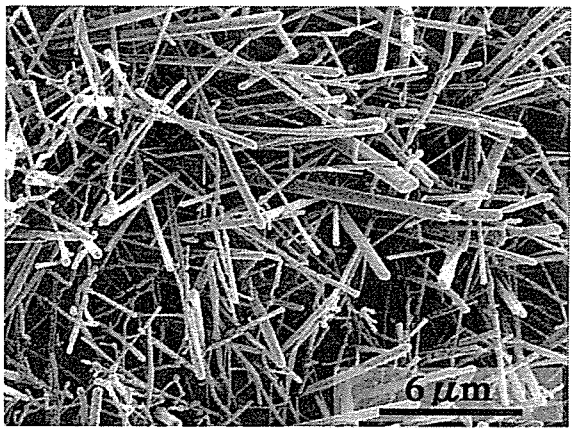

Fig.2 SEM image of the microstructure of β-TCP granules obtained by sintering at 900 °C from HA granules prepared by hydrothermal treatment at 160 °C.

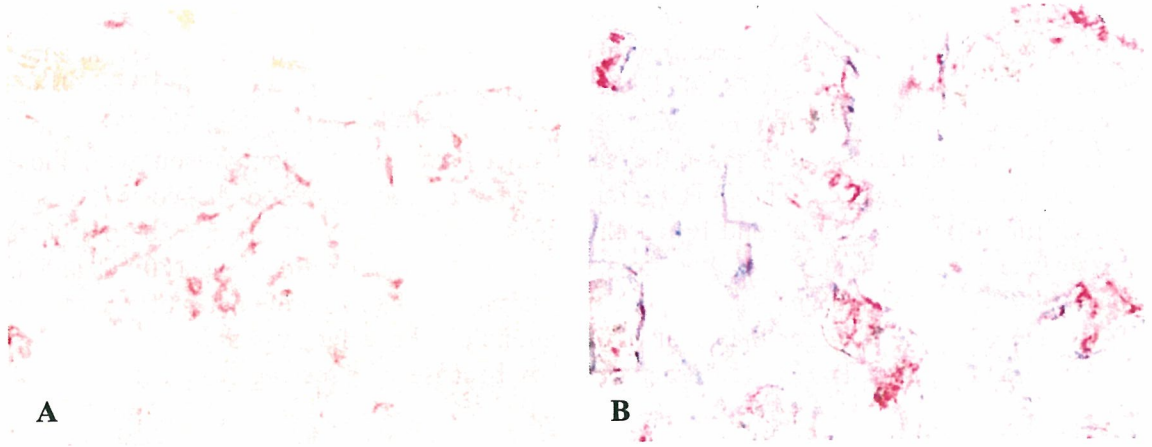

Fig.2 (A)Representative photomicrograph of the TRAP-positive multinucleated osteoclasts and new bone formation on the margin of the RSβ-TCP implant, 3 weeks after grafting. (TRAP, x100)
(B)Representative photomicrograph of the RSβ-TCP implant 24 weeks after grafting. Numerous TRAP-positive multinucleated osteoclasts and new prominent bone formation. (TRAP,x100)

Three weeks after grafting, absorption of HA implants was not remarkably observed. TRAP-positive multinucleated osteoclasts were seen in the specimens, but the number was much less than that in the specimens grafted RSβ-TCP (Fig.3A). Twenty-four weeks after grafting, absorption of HA was still unremarkable, and in contrast to the specimens grafted RSβ-TCP, original margins of the HA implants were clearly recognized. Number of TRAP-potisive multinucleated osteoclasts was also much less than that in the specimens grafted RSβ-TCP (Fig.3B). Bone formation was observed in the specimens grafted HA, but it was restricted in the holes created in the implant (Fig.4).
These results showed that biodegradation of RSβ-TCP was nicely accompanied with new bone formation, and suggested that RSβ-TCP was metabolized like normal bone tissue.

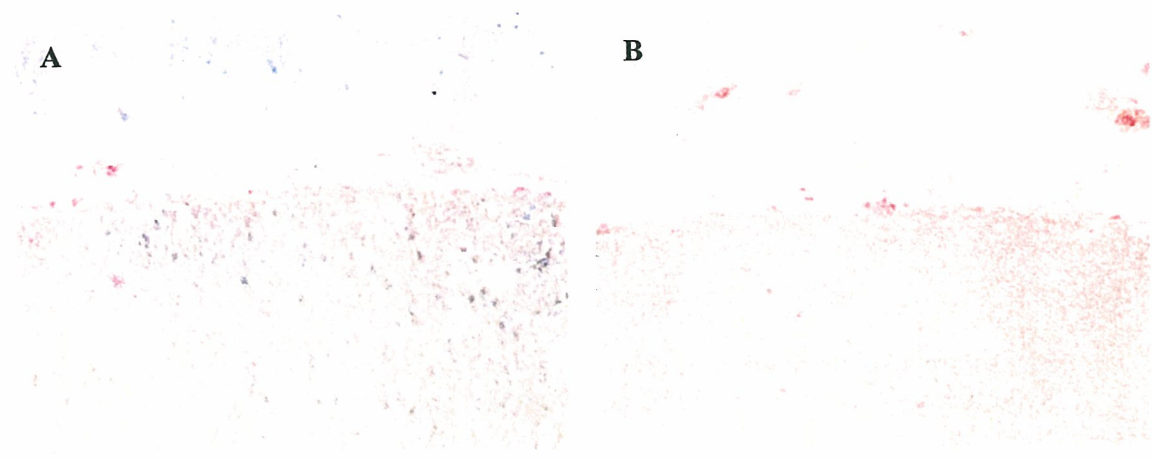

Fig.3 Representative photomicrographs of the TRAP-positive multinucleated osteoclasts on the margin of the HA implants, (A) 3 weeks after grafting and (B) 24 weeks after grafting. (TRAP,x100)

Calcium deficient HA tends to decompose easily into tricalcium phosphates by heating in comparison with stoichiometric HA [8, 9]. Thus, porous granules of β-TCP were obtained from the porous granules of calcium deficient HA with Ca/P ratio of 1.50 by heating them at 900 °C for 3 h in air. The β-TCP granules had almost the same micro-structure in comparison with the HA granules before heating (Fig.1). The β-TCP granules were composed of rod-shaped particles with about 10-20 μm in length (Fig.2), and it had almost same porosity as the samples before heating. Specific surface area of β-TCP granules prepared hydrothermal treatment at 160 °C and then sintering at 900 °C was about 7 $m^2 \cdot g^{-1}$ by BET measurement. The mean diameter of micro-pore of β-TCP granules was slight larger than that of HA granules, the value was about 0.2 μm in size (Fig.3). The granules of β-TCP were harder than HA because of sintering which made bonding among particles.

Porous β-TCP with much amount of micro-pores prepared in this study should be more bio-degradable than the conventional materials. These porous granules must be suitable for the bone graft material and the scaffold of cultured bone. It is considered that the implant *in vivo* is probably first coated with plasma proteins and blood coagulation materials before cells adhesion take place, therefore micro-pores must effect the osteointegration process because such pores are similar in size to that of proteins. The micro-pores must make the protein adhesion to the materials surface [10].

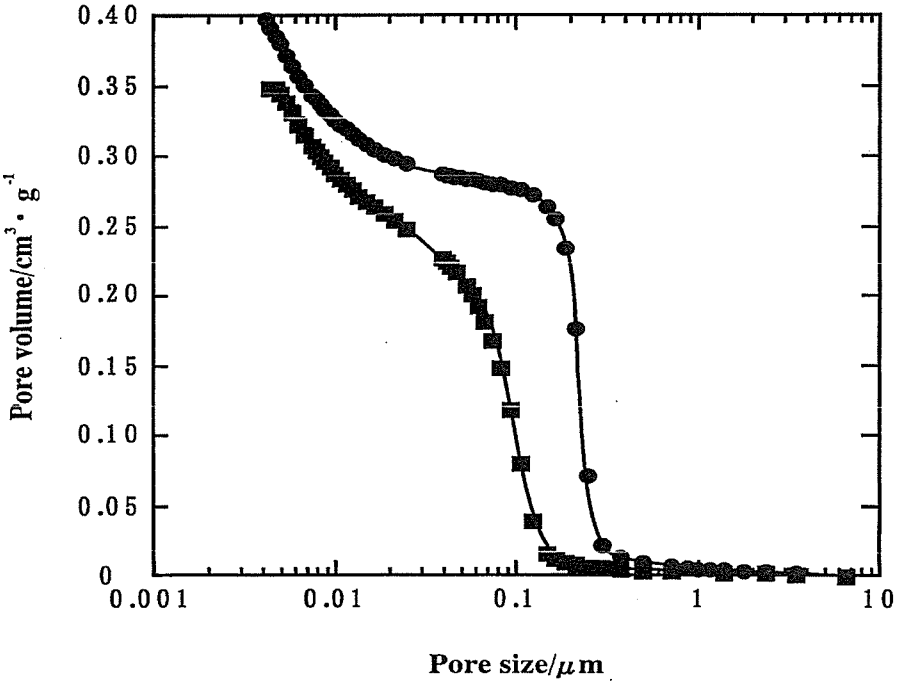

Fig.3 Pore size distribution of granules of hydroxyapatite (■) prepared by hydrothermal treatment at 160 °C and β-tricalcium phosphate (●) prepared from this hydroxyapatite.

Summary

Porous granules of β-tricalcium phosphate with about 40 %-60 % porosity were prepared from the porous granules of calcium deficient hydroxyapatite by heating them at 900 °C for 3 h in air. These granules were composed of rod-shaped particles of about 10-20 μm in length, and had much amount of micro-pores of about 0.1-0.5 μm in size. The micro-pores can be filled with proteins. The porous granules of β-TCP must be suitable for the bone graft material and for scaffold of cultured bone.

Acknowledgement
The present research was supported by the Grant-in-Aid for Scientific Research ((C)16560592) and ((C)17630008) from the Japan Society for the Promotion of Science.

References

[1] H. U. Cameron, I. Macnab and R. M. Pilliar, J. Biomed. Mater. Res., Vol. 11 (1977), p. 179
[2] S. F. Hulbert, F. A. Young, R. S. Mathews, J. S. Klawitter, C. D. Talbert and F. H. Stelling, J. Biomed. Mater. Res., Vol. 4 (1970) p. 433
[3] K. Ioku, S. Goto, H. Kurosawa, K. Shibuya, H. Yokozeki, T. Hayashi and T. Nakagawa, Phosp. Res. Bull., Vol. 7 (1997), p. 29
[4] H. Yokozeki, T. Hayashi, T. Nakagawa, H. Kurosawa, K. Shibuya and K. Ioku, J. Mater. Sci.: Mater. Med., Vol. 9 (1998), p. 381
[5] K. Ioku, M. Toda, H. Fujimori, S. Goto and M. Yoshimura: Key Engineering Materials Vol. 254-256, (2004), p. 19
[6] K. Ioku, M. Fukuhara, H. Fujimori and S. Goto, Korean J. Ceram., Vol. 5 (1999), p.115
[7] M. Yoshimura, H. Suda, K. Okamoto and K. Ioku: J. Mater. Sci. Vol. 29 (1994), p. 3399
[8] K. Ioku, T. Murakami, Y. Ikuma and M. Yoshimura, J. Ceram. Soc. Japan, Int. Edition, Vol. 100 (1992), p.1001
[9] K. Ishikawa, P. Ducheyne and S. Radin, J. Mater. Sci.: Mater. Med., Vol. 4 (1993), p. 165
[10] V. S. Komlev and S. M. Barinov, J. Mater. Sci.: Mater. Med., Vol. 13 (2002), p. 295

Key Engineering Materials Vols. 309-311 (May 2006) pp. 1063-1066

Porous Ceramics of β-tricalcium Phosphate Composed of Rod-shaped Particles is Highly Biodegradable and Expresses Prominent Osteoconductivity

Takatoshi Okuda[1, 2, a], Ikuho Yonezawa[2, b], Koji Ioku[3, c], Hideyuki Minagi[4, d], Hisashi Kurosawa[2, e] and Tohru Ikeda[1, f]

[1]Division of Oral Pathology and Bone Metabolism, Department of Developmental and Reconstructive Medicine, Nagasaki University Graduate School of Biomedical Sciences, 1-7-1 Sakamoto, Nagasaki 852-8588, Japan

[2]Department of Orthopedic Surgery, School of Medicine, Juntendo University, 2-1-1 Hongo, Tokyo 113-8421, Japan

[3]Graduate School of Environmental Studies, Tohoku University, 6-6-20 Aoba, Sendai 980-8579, Japan

[4]Technical Research Laboratory, Toyo Kohan Co., Ltd., Kudamatsu, Yamaguchi 744-8611, Japan

[a]f1930@cc.nagasaki-u.ac.jp, [b]yoza@med.juntendo.ac.jp, [c]ioku@mail.kankyo.tohoku-u.ac.jp, [d]u5812@toyokohan.co.jp, [e]kuro@med.juntendo.ac.jp , [f]tohrupth@net.nagasaki-u.ac.jp

Keywords: Beta tricalcium phosphate, Hydroxyapatite, Bone graft

Abstract. Newly developed porous β-tricalcium phosphate composed of rod-shaped particles was grafted into distal end of the left femur of female Japan White rabbit. As a control, hydrixyapatite generated in the same size was grafted. In both implants, 350μm in diameter-sized holes were created vertically and horizontally. Three weeks after grafting, margin of the β-tricalcium phosphate was absorbed by osteoclasts and bone formation was seen near the absorbed region. Twenty-four weeks after grafting, more than 80% of the β-tricalcium phosphate was absorbed and newly formed bone was prominently observed. The hydroxyapatite was not remarkably absorbed even 24 weeks after grafting, and newly formed bone was observed only in the holes created in the implants. These results suggest that porous β-tricalcium phosphate composed of rod-shaped particles has highly biodegradable and osteoconductive nature, and appropriate to bone graft substitute.

Introduction

Autogenous bone grafts are frequently used for the treatment of the large bone defects. Bone harvesting can induce postoperative complications and sometimes can not provide a sufficient quantity of bone. Therefore, synthetic biomaterials have been investigated as an alternative to autogenous bone grafts.Beta tricalcium phosphate (β-TCP) has been shown to have osteoconductivity and biodegradable nature in animal experiments and in human bones [1-3]. However, the bio-resorption and osteoconductivity are insufficient compared to those of grafted bone, and further efforts including tissue engineering have been tried [4,5]. We recently developed new porous ceramics of β-TCP composed of rod-shaped particles (RSβ-TCP) [6] (Fig.1). In this study, we grafted RSβ-TCP or hydroxyapatite (HA) in rabbit femurs, and compared the osteoconductivity and biodegradable nature.

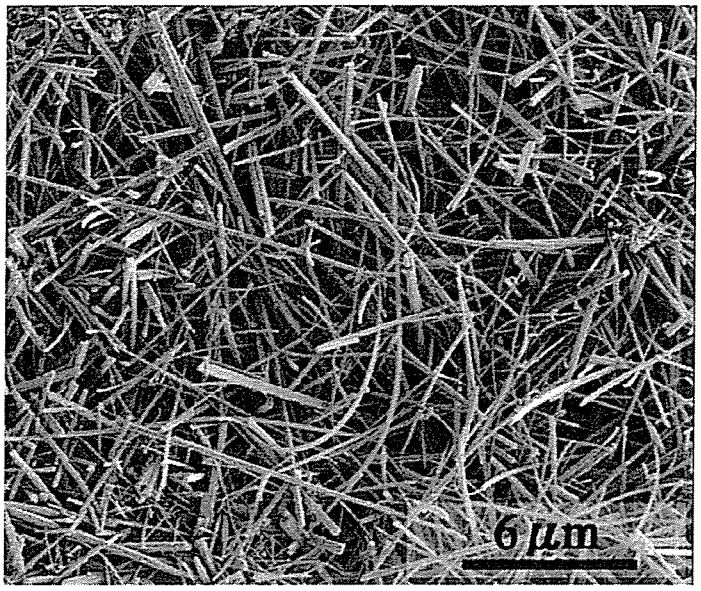

Fig.1 Scanning electron micrograph of the RSβ-TCP surface

Materials and Methods

RSβ-TCP implants (6 mm in diameter and 10 mm in length) were prepared using α-tricalcium phosphate powder and 50-75 mass% glycine particles of about 100-200μm in size. The samples were set in a 105 cm^3 autoclave with 10 cm^3 of dilute aqueous ammonia, exposed to vapor of the solution under the saturated vapor pressure for 20h and heated at 900 ℃ for 3h in air (Arch. Bioceram. Res. 4:121-124, 2004). HA implants in the same size were prepared by normal sintering method. In both implants, 350 μm in diameter-sized holes were created vertically and horizontally, and served for test implants.In the distal end of the left femur of female Japan White rabbit weighing 2.5 kg, 6 mm diameter-sized dead-end defect was created, each test implant was inserted into the defect and soft tissues were closed. Three weeks or 24 weeks after grafting, the rabbits were sacrificed, the tissue specimens were fixed in 4% formaldehyde in 0.1M phosphate buffer (pH 7.2), embedded in 2-hydroxyethyl methacrylate/methyl methacrylate/2-hydroxyethyl acrylate mixed resin and 3μm thick sections were made. These sections were stained with toluidine blue or tartrate-resistant acid phosphatese (TRAP) activity was analyzed histochemically.

Results and Discussion

Three weeks after grafting, absorption of RSβ-TCP began to be seen. The absorption occurred on the margin of the implant and around the holes created in the implant. On the surface of the absorbed RSβ-TCP, TRAP-positive multinucleated osteoclasts were seen and the absorption was thought to be madiated by osteoclasts. Bone formation was also seen in the holes created in the implant and space formed by absorption of the implant. Cuboidal active osteoblasts, osteoid and mineralized bone were seen in these regions (Fig.2A). Twenty-four weeks after grafting, more than 80% of RSβ-TCP was absorbed. Numerous TRAP-positive multinucleated osteoclasts were seen and the remaining RSβ-TCP was expected to be absorbed before long. Numerous cuboidal active osteoblasts were also seen and the amount of newly formed bone was significantly increased in comparison to the specimens 3 weeks after grafting. Original margins of the implants were no longer recognized because of prominent absorption of RSβ-TCP and bone formation (Fig.2B).

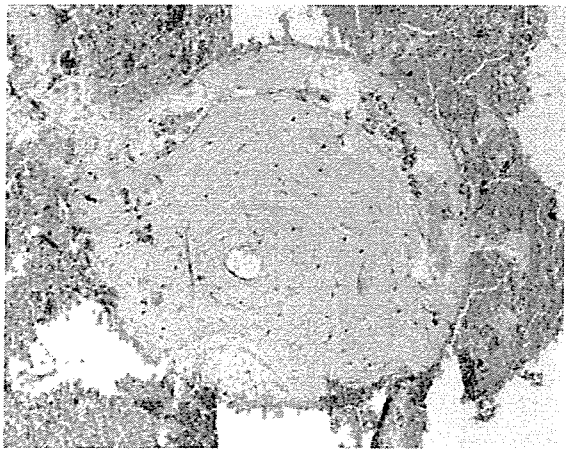

Fig.4 Bone formation observed only in the holes of the HA implant 24 weeks after grafting. (HE, x100)

References

[1] A. Ogose, T. Hotta, H. Hatano, H. Kawashimia, K. Tokunaga, N. Endo and H. Umezu: J. Biomed. Mater. Res., 63, 601-604 (2002).

[2] C. J. Anker, S. P. Holdridge, B. Baird, H. Cohen and T. A. Damron: Clin. Orthopaed. Rel. Res., 434, 251-257 (2005).

[3] N. Kondo, A. Ogose, K. Tokunaga, T. Ito, K. Arai, N. Kudo, H. Inoue and N. Endo: Biomaterials, 26, 5600-5608 (2005).

[4] T. Uemura, J. Dong, Y. Wang, H. Kojima, T. Saito, D. Iejima, M. Kikuchi, J. Tanaka and T. Tateishi: Biomaterials, 24, 2277-2286 (2003).

[5] N. Matsushita, H. Terai, T. Okada, K. Nozaki, H. Inoue, S. Miyamoto and K. Takaoka: J. Biomed. Mater. Res. 70A, 450-458 (2004).

[6] K. Ioku, H. Minagi, I. Yonezawa, T. Okuda, H. Kurosawa, T. Ikeda, H. Misumi, K. Nakahara, H. Fujimori and S. Goto: Arch. Bioceram. Res. 4, 121-124 (2004).

The Journal of Toxicological Sciences,
Vol.31, No.5, 433-448, 2006

UTILIZATION OF A ONE-DIMENSIONAL SCORE FOR SURVEYING CHEMICAL-INDUCED CHANGES IN EXPRESSION LEVELS OF MULTIPLE BIOMARKER GENE SETS USING A LARGE-SCALE TOXICOGENOMICS DATABASE

Naoki KIYOSAWA[1], Kouji SHIWAKU[1], Mitsuhiro HIRODE[1], Ko OMURA[1], Takeki UEHARA[1], Toshinobu SHIMIZU[1], Yumiko MIZUKAWA[2], Toshikazu MIYAGISHIMA[1], Atsushi ONO[1], Taku NAGAO[3] and Tetsuro URUSHIDANI[1,2]

[1]*Toxicogenomics Project, National Institute of Biomedical Innovation, 7-6-8 Asagi, Ibaraki, Osaka 567-0085, Japan*

[2]*Department of Pathophysiology, Faculty of Pharmaceutical Sciences, Doshisha Women's College of Liberal Arts, Kodo, Kyotanabe, Kyoto 610-0395, Japan*

[3]*National Institute of Health Sciences, 1-18-1 Kamiyoga, Setagaya-ku, Tokyo 158-8501, Japan*

(Received August 18, 2006; Accepted September 11, 2006)

ABSTRACT — A large-scale toxicogenomcis database has now been constructed in the Toxicogenomics Project in Japan (TGP). To facilitate the analytical procedures for such large-scale microarray data, we developed a simple one-dimensional score, named TGP1 which expresses the trend of the changes in expression of biomarker genes as a whole. To evaluate the usefulness of the TGP1 score, microarray data of rat liver and rat hepatocytes deposited in the TGP database were scored for three biomarker gene sets, i.e., carcinogenesis-related, PPARα-regulated and glutathione depletion-related gene sets. The TGP1 scoring system gave reasonable results, i.e., the scores for carcinogenesis-related genes were high in omeprazole-, chlorpromazine-, hexachlorobenzene-, sulfasalazine- and Wy-14,643-treated rat livers, that for PPARα-regulated genes were high in clofibrate-, Wy-14,643-, gemfibrozil-, benzbromarone- and aspirin-treated rat livers as well as rat hepatocytes, and for glutathione deficiency-related genes were high in omeprazole-, bromobenzene-, acetaminophen- and coumarin-treated rat liver. We concluded that the TGP1 score is useful for surveying the expression changes in multiple biomarker gene sets for a large-scale toxicogenomics database, which would reduce the time of doing conventional multivariate statistical analysis. In addition, the TGP1 score can be applied to screening of compatible biomarker gene sets between rat liver and rat hepatocytes, like PPARα-regulated gene sets, which will allow us to develop an appropriate in vitro system for drug safety assessment in vivo.

KEY WORDS: Toxicogenomics, Database, Scoring system, Liver, Rat

INTRODUCTION

Toxicogenomics has been considered to be a promising methodology for understanding the molecular mechanisms of toxicity, and this has been proven by a number of studies (Kiyosawa *et al.*, 2004b; Sehata *et al.*, 2004; Ito *et al.*, 2006). Toxicogenomics research requires a high-quality microarray database that covers a sufficient number of well-studied compounds, and such databases are being developed for both public and commercial use (Boverhof and Zacharewski, 2006). The Toxicogenomics Project in Japan (TGP) has been conducted by the collaborative research of 15 pharmaceutical companies, the National Institute of Health Science and the National Institute of Biomedical Innovation, and is a five-year project started from 2002 (Takashima *et al.*, 2006; Urushidani and Nagao, 2005). The TGP database is a toxicogenomics-oriented data-

Correspondence: Tetsuro URUSHIDANI (E-mail: turushid@dwc.doshisha.ac.jp)

base that consists of microarray data of rat liver, rat hepatocytes and human hepatocytes, as well as traditional toxicological data for 150 compounds. The large-scale TGP database is expected to be useful for characterizing the chemical-induced molecular dynamics and for evaluating and predicting the potential risk of chemical toxicity at early stages of drug development.

Specific gene sets whose mRNA levels are correlated with certain toxicological phenotypes, or toxicogenomics biomarkers, are useful for evaluating the toxicological significance from microarray data. For example, previous reports demonstrated that certain gene sets could be applied for evaluating a chemical-induced glutathione deficiency or risk of acetaminophen-type hepatotoxicity (Kiyosawa *et al.*, 2004a), a chemical-induced phospholipidosis not only in rodent but also in the human case (Sawada *et al.*, 2005), and evaluation of the carcinogenic potential of the chemicals (Ellinger-Ziegelbauer *et al.*, 2004). Such candidate biomarkers have been rapidly accumulated. The significance of the toxicogenoimics database will grow synergistically with accumulation of toxicogenomics biomarker information.

When using the toxicogenomics database, one of the major obstacles is its gigantic data size. Furthermore, it becomes more complex as the toxicogenomics biomarker knowledge accumulates. Multivariate statistical techniques such as hierarchical clustering, k-means clustering, self-organizing map or principal component analysis are usually applied for analyzing the microarray data (Kaminski and Friedman, 2002; Draghici, 2003). Although such techniques provide the general characteristics of gene expression profiles rather intuitively, they are not suitable for high-throughput analysis when a series of biomarker gene sets is to be analyzed at the same time. One simple solution is to circumvent the time-consuming analytical procedure by utilizing a one-dimensional score, which reflects the level of gene expression changes for certain biomarker gene sets. The calculated scores for many samples can be presented in the multiple biomarker gene sets simultaneously, so it becomes easy to capture the toxicological endpoints that should be focused on for further detailed analysis. In the present study, we have developed a score that reflects the level of chemical-induced gene expression changes for certain biomarker gene sets in our large-scale TGP database. The score is calculated from the fold change value of each gene, calculated by dividing the mean signal of the chemical-treated group by that of the vehicle-treated group, and therefore is easy to calculate and interpret results. The usefulness of the presented score was verified in three biomarker gene sets.

MATERIALS AND METHODS

Chemicals

Thirty-eight chemicals used for the data analysis are listed in Table 1, in which the chemical name, manufacturer, highest dosage and vehicle used in the study are described. In our standard protocol, all the drugs were administered in three dose levels, i.e., high, middle (1/3 of the high dose), and low (1/10 of the high dose). In the present study, however, the data of the high dose are exclusively shown for simplicity. In certain cases (Fig. 3), the results of other dose levels are also exhibited in order to show dose-dependency.

Animal treatment

Six-week old male Sprague-Dawley rats (Charles River Japan, Inc., Kanagawa, Japan) consisted of five animals per group and were used for the in-life study. The detailed study information is the same as in the literature (Takashima *et al.*, 2006). Rats were sacrificed at 24 hr after a single dosing of chemicals. Liver was removed at necropsy, and soaked in RNAlater® (Ambion Inc., Austin, TX, USA) to prevent RNA degradation. We affirm that experimental protocols for both the animal and hepatocyte studies were reviewed and approved by the Ethics Review Committee for Animal Experimentation of the National Institute of Health Science.

Hepatocytes treatment

Hepatocytes were isolated from 6-week-old male Sprague-Dawley rats under sodium pentobarbital (120 mg/kg, ip) and anesthetized by a modified two-step collagenase perfusion method. The liver was perfused via the portal vein for 10 min with divalent cation-free, EGTA (0.5 mM)-supplemented HEPES buffered Hank's balanced salt solution followed by a 10-min perfusion with HEPES (10 mM)-buffered normal Hank's balanced salt solution containing soybean trypsin inhibitor (Sigma, T-2011, 0.05 g/L) and collagenase (WAKO 034-10533, 0.5 g/L) at the flow rate of 10 - 30 ml/min. The isolated cells were washed three times by 50 g for 1 min to obtain a parenchymal cell-enriched pellet. Hepatocytes were not used when their viability assessed by trypan blue exclusion was lower than 70%. The cells were seeded into collagen-coated six-well plates (BD BioCoat™ Collagen I Cellware,

Table 1. Chemicals.

ID	Chemicals (abbreviation)	Manufacturer	*in vivo*		*in vitro*	
			Dosage (mg/kg)	Vehicle	Concentration (μM)	Vehicle
001	Acetaminophen (APAP)	Sigma-Aldrich	1000	MC	10000	Medium
002	Isoniazid (INAH)	Sigma-Aldrich	200	MC	10000	Medium
003	Carbon tetrachloride	Sigma-Aldrich	300	OIL	10000	DMSO
004	Phenobarbital	Sigma-Aldrich	100	MC	10000	Medium
005	Valproate sodium (VPA)	Wako Pure Chemical Industries, Ltd.	450	MC	5000	Medium
006	Clofibrate	Wako Pure Chemical Industries, Ltd.	300	OIL	300	DMSO
007	Methotrexate	Wako Pure Chemical Industries, Ltd.	100	MC	3000	Medium
008	Rifampicin	Wako Pure Chemical Industries, Ltd.	200	MC	70	DMSO
009	Alpha-naphthy lisothiocyanate (ANIT)	Kanto Chemical Co., Inc.	15	OIL	200	DMSO
010	Allyl alcohol	Tokyo Chemical Industry Co., Ltd	30	OIL	70	Medium
011	Phenylbutazone	Sigma-Aldrich	200	MC	400	DMSO
012	Omeprazole (OPZ)	Wako Pure Chemical Industries, Ltd.	1000	MC	600	DMSO
013	Ethionine (ET)	Tokyo Chemical Industry Co., Ltd	250	MC	10000	Medium
014	Aspirin (ASA)	Wako Pure Chemical Industries, Ltd.	450	MC	3000	DMSO
015	Indomethacin	Sigma-Aldrich	5	MC	200	DMSO
016	Chlorpromazine (CPZ)	Wako Pure Chemical Industries, Ltd.	45	MC	20	DMSO
017	Thioacetamide	Sigma-Aldrich	45	MC	10000	Medium
018	Carbamazepine	Sigma-Aldrich	300	MC	300	DMSO
019	Diclofenac sodium (DFNa)	CAYMAN / Tokyo Chemical Industry Co., Ltd.	10	MC	400	DMSO
020	Nitrofurantoin	ICN	100	MC	125	DMSO
021	Benzbromarone (BBr)	Sigma-Aldrich	200	MC	100	DMSO
022	Hexachlorobenzene (HCB)	Tokyo Chemical Industry Co., Ltd	300	OIL	30	DMSO
023	Diazepam	Wako Pure Chemical Industries, Ltd.	250	MC	250	DMSO
024	Cyclophosphamide	Sigma-Aldrich	15	MC	2000	Medium
025	Methapyrilene hydrochloride	Sigma-Aldrich	100	MC	600	Medium
026	Phenytoin	Tokyo Chemical Industry Co., Ltd	600	MC	300	DMSO
027	Coumarin (CMA)	Tokyo Chemical Industry Co., Ltd	150	OIL	300	DMSO
028	Allopurinol	Sigma-Aldrich	150	MC	140	DMSO
029	Propylthiouracil	Tokyo Chemical Industry Co., Ltd	100	MC	4000	Medium
030	Wy-14,643 (WY)	Tokyo Chemical Industry Co., Ltd	100	OIL	150	DMSO
031	Gemfibrozil (GFZ)	Sigma-Aldrich	300	OIL	100	DMSO
032	Bromobenzene (BBz)	Tokyo Chemical Industry Co., Ltd	300	OIL	200	DMSO
033	Amiodarone hydrochloride	Sigma-Aldrich	200	MC	7	DMSO
034	Sulfasalazine (SS)	Sigma-Aldrich	1000	MC	150	DMSO
035	Cimetidine	Tokyo Chemical Industry Co., Ltd	1000	MC	300	DMSO
042	Glibenclamide	Sigma-Aldrich	1000	OIL	20	DMSO
045	Perhexiline maleate	Sigma-Aldrich	150	MC	15	DMSO
046	Azathioprine	ICN	30	MC	75	DMSO

BD Bioscience) at a density of 1×10^6 cells/well in 2 ml HMC Bulletkit medium (CAMBREX) supplemented with 10% fetal bovine serum. Following an attachment period of 3 hr, the medium was replaced and kept overnight before drug exposure at 37°C in an atmosphere of 5% CO_2. The test compounds were added to the medium directly or as a 1000× stock solution in dimethylsulfoxide (DMSO). After 2, 8 and 24 hr-exposure, cells were dissolved with RLT buffer (Qiagen) and collected for expression profiling. GeneChip analysis was performed in a duplicated manner for each time and concentration point.

Microarray analysis

The detailed information is described in the previous literature (Takashima *et al.*, 2006). Briefly, 3 liver samples out of 5 samples collected in the animal were used for analysis. Total RNA was isolated using RNeasy Mini Kit with Bio Robot 3000 (Qiagen, Inc., Valencia, CA, USA), and 5 μg of the total RNA was used for cDNA synthesis using T7-(dT)24 oligonucleotide primer (Affymetrix, Inc., Santa Clara, CA, USA) and SuperScript Choice System (Invitrogen, Carlsbad, CA, USA). Biotin-labeled cRNA was synthesized using BioArray High Yield RNA Transcription Labeling Kit (Enzo Diagnostics, Farmingdale, NY, USA). The hybridization cocktail was prepared with 10 μg of fragmented cRNA, and hybridized to RAE 230A GeneChip array (Affymetrix, Inc.) at 45°C for 18 hr. The hybridized GeneChip array was washed and stained by streptavidin-phycoerythrin using Fluidics Station 400 (Affymetrix, Inc.) and scanned by GeneArray Scanner (Affymetrix, Inc.). The scanned image files were analyzed using Microarray Suite ver. 5.0. All the microarray data were scaled by global normalization where the mean signal intensity of each data was adjusted to 500. A heat map representing gene expression levels was created using Spotfire software (Spotfire, Inc., Somerville, MA).

Biomarker gene sets

Three lists of probe sets of RG U34A arrays are selected from the literature whose signals were reported to be increased by certain chemical treatments: i) carcinogenicity-related gene probe sets (Ellinger-Ziegelbauer *et al.*, 2004), ii) PPARα-regulated gene probe sets (Richert *et al.*, 2003), and iii) glutathione deficiency-correlated gene probe sets (Kiyosawa *et al.*, 2004a). The information for the selected probe sets is summarized in Table 2, and lists of the probe sets for each biomarker gene set are presented from Table 3 to Table 5. Since the selected probe sets were those of RG U34A array, the corresponding probe sets of RAE 230A array were determined by selecting "good match probe sets", where the probe sets whose corresponding probe sequences do not overlap between those of RG U34A and RAE 230A array were removed. The "good match probe set" information is provided in the NetAffx Website (Liu *et al.*, 2003).

Calculation of TGP1 score

The TGP1 score was calculated as shown in Fig. 1. Signal log ratio was calculated by dividing the mean signal value of the chemical-treated group by that of corresponding control. First, the sum of the signal log ratios for the used probe sets was calculated, and then divided by the number of probe sets used (Index 1). Next, the sum of squared signal log ratios for the used probe sets was calculated, and then divided by the number of probe sets used (Index 2). Finally, the TGP1 score was calculated by multiplying Index 1 with Index 2.

Individual gene expression analysis

The fold change in carcinogenesis- and glutathione deficiency-related genes is calculated by dividing signal data of the chemical-treated group by mean signal data (n=3 for rat liver and n=2 for rat hepatocytes) of corresponding control. The signal log ratio

Table 2. Summary of biomarker gene sets used in the present study.

Biomarker	Number of probe sets RG U34A	RAE 230A	Reference
Carcinogenicity-related	55	26	Ellinger-Ziegelbauer *et al.*, 2004
PPARα-regulated	30	17	Richert *et al.*, 2003
Glutahione deficiency-related	69	45	Kiyosawa *et al.*, 2004

Three biomarker gene sets whose expression levels were reported to be increased by carcinogens, PPARα activators or glutathione depletors, were selected from the literature, and used for calculation of the TGP1 score. These genes were originally identified using a RG U34A GeneChip array, and the corresponding "good match" probe sets of the RAE 230A GeneChip array were re-selected according to the information provided by the NetAffx website.

Scoring the level of gene expression changes in microarray analysis.

Table 3. Carcinogenesis-related gene probe sets.

Affymetrix probe set ID		
RG U34A	RAE 230A	Gene name
X62952_at	1367574_at	Vimentin
L13039_s_at	1367584_at	Annexin A2
M58404_at	1367655_at	Thymosin, beta 10
X13044_at	1367679_at	CD74 antigen
rc_AI169327_at	1367712_at	Tissue inhibitor of metalloproteinase 1
D10729_s_at	1367786_at	Proteosome subunit, beta type 8
M32062_at	1367850_at	Fc receptor, IgG, low affinity III
M34253_at	1368073_at	Interferon regulatory factor 1
AF045464_s_at	1368121_at	Aldo-keto reductase family 7, member A3
M76704_s_at	1368311_at	*O*-6-Methylguanine-DNA methyltransferase
U62940_at	1368552_at	GrpE-like 1
U10894_s_at	1368558_s_at	Allograft inflammatory factor 1
AB010635_s_at	1368905_at	Carboxylesterase 2
U73174_g_at	1369061_at	Glutathione reductase
M31038_at	1369110_x_at	RT1 class Ib, locus Aw2
L12138_at	1369499_at	Thymidylate synthase
D42148_at	1369735_at	Growth arrest specific 6
U02322_s_at	1369783_a_at	Neuregulin 1
rc_AA900505_at	1369958_at	RhoB gene
X60351cds_s_at	1370026_at	Crystallin, alpha B
AJ011969mRNA_at	1370153_at	Growth differentiation factor 15
D10757_at	1370186_at	Proteosome subunit, beta type 9
E00717UTR#1_s_at	1370269_at	CYP1A1
U66470_at	1370361_at	Cell growth regulator with EF hand domain 1
M81855_at	1370583_s_at	ATP-binding cassette, sub-family B (MDR/TAP), member 1
J05181_at	1370688_at	Glutamate-cysteine ligase, catalytic subunit
AF084186_s_at	1370838_s_at	Alpha-spectrin 2
M15562_at	1370883_at	RT1 class II, locus Da
Z12298cds_s_at	1370956_at	Decorin
X56596_at	1371033_at	RT1 class II, locus Bb
S72506_s_at	1371089_at	Glutathione S-transferase Yc2 subunit
M63991_at	1371143_at	Serine (or cysteine) peptidase inhibitor, clade A, member 7
X75207_s_at	1371150_at	Cyclin D1
X51707cds_s_at	1371377_at	Ribosomal protein S19
rc_AI639488_at	1384427_at	Transformed mouse 3T3 cell double minute 2 (predicted)
AF083269_at	1386925_at	Actin-related protein 2/3 complex, subunit 1B
M60921_at	1386994_at	B-cell translocation gene 2, anti-proliferative
L03201_at	1387005_at	Cathepsin S
rc_AA875455_at	1387021_at	Wild-type p53-induced gene 1
AF001898_at	1387022_at	Aldehyde dehydrogenase family 1, member A1
U24174_at	1387391_at	Cyclin-dependent kinase inhibitor 1A
J02679_s_at	1387599_a_at	NAD(P)H dehydrogenase, quinone 1
M26125_at	1387669_a_at	Epoxide hydrolase 1
U17035_s_at	1387969_at	Chemokine (C-X-C motif) ligand 10
X57523_at	1388149_at	Transporter 1, ATP-binding cassette, sub-family B (MDR/TAP)
rc_AA893246_at	1388325_at	ATPase, H+ transporting, V1 subunit D
rc_AA944397_at	1388850_at	Heat shock protein 1, alpha

Table 3. Continued.

U49729_at	none	–
X70871_at	none	–
S56936_s_at	none	–
D38062exon_s_at	none	–
M17412_at	none	–
X59375mRNA_at	none	–
rc_AA894027_at	none	–
rc_AA945082_at	(1371089_at)	–

Probe sets whose signals are reported as increased by treatment of carcinogens in RG U34A GeneChip analysis were selected from the previous literature, and the corresponding probe sets of RAE 230A GeneChip were determined by referring to "good match probe sets" information provided by Affymetrix. Seven probe sets of RG U34A GeneChip did not show any corresponding probe sets in RAE 230A GeneChip, and were presented as "none" in the table. S72506_s_at and rc_AA945082_at are redundant probe sets of RG U34A GeneChip for 1371089_at probe set in RAE 230A GeneChip.

Table 4. PPARα-regulated gene probe sets.

Affymetrix probe set ID		
RG U34A	RAE 230A	Gene name
J02752_at	1367680_at	Acyl-Coenzyme A oxidase 1
AF072411_g_at	1367689_a_at	CD36 antigen
D43623_g_at	1367742_at	Carnitine palmitoyltransferase 1b
K03249_at	1368283_at	Enoyl-Coenzyme A, hydratase/3-hydroxyacyl Coenzyme A dehydrogenase
M57718mRNA_s_at	1368934_at	CYP4A10
V01235_at	1369111_at	Fatty acid binding protein 1, liver
X65296cds_s_at	1370363_at	Carboxylesterase 3
AF044574_g_at	1370818_at	2-4-Dienoyl-Coenzyme A reductase 2
rc_AA893239_at	1371012_at	2-Hydroxyphytanoyl-Coenzyme A lyase
L00320cds_f_at	1371076_at	CYP2B2
U08976_at	1386885_at	Enoyl coenzyme A hydratase 1
rc_AA946368_at	1386901_at	Similar to CD36 antigen
M21208mRNA_s_at	1387123_at	CYP17A1
J02749_g_at	1387783_a_at	Acetyl-Coenzyme A acyltransferase 1
Y09333_g_at	1388210_at	Acyl-CoA thioesterase 1
AB010428_s_at	1398250_at	Acyl-CoA thioesterase 1
AB005743_g_at	none	–
rc_AA924267_s_at	none	–
X07259cds_s_at	none	–
rc_AA925752_at	none	–
K01721mRNA_s_at	none	–
M14972_i_at	none	–
X72792cds_s_at	none	–
rc_AA799489_g_at	none	–
AF072411_at	(1367689_a_at)	–
L46791_at	(1370363_at)	–
J00728cds_f_at	(1371076_at)	–
M11251cds_f_at	(1371076_at)	–
J02749_at	(1387783_a_at)	–
Y09333_at	(1388210_at)	–

Probe sets whose signals are reported to be increased by treatment of PPARα activators in the RG U34A GeneChip analysis were selected from the literature, and the corresponding probe sets of RAE 230A GeneChip were determined by referring to "good match probe sets" information provided by Affymetrix. Eight probe sets of RG U34A GeneChip did not show any corresponding probe sets in RAE 230A GeneChip, and were presented as "none" in the table. Six probe sets of RG U34A GeneChip had redundant probe sets for the same genes, and the corresponding probe sets are presented in brackets in the table.

Scoring the level of gene expression changes in microarray analysis.

Table 5. Glutathione deficiency-related gene probe sets.

Affymetrix probe set ID		
RG U34A	RAE 230A	Gene name
rc_AI231807_at	1367559_at	Ferritin light chain
M29358_g_at	1367573_at	Ribosomal protein S6
J02752_at	1367680_at	Acyl-Coenzyme A oxidase 1
X78848cds_f_at	1367774_at	Glutathione *S*-transferase A5
M64733mRNA_s_at	1367784_a_at	Clusterin
AF026554_at	1367815_at	Solute carrier family 5, member 6
rc_AA892821_at	1367843_at	Aldo-keto reductase family 7, member A2
Y17295cds_s_at	1367969_at	Peroxiredoxin 6
U04733_s_at	1367988_at	CYP2C23
M57428_s_at	1368116_a_at	Ribosomal protein S6 kinase, polypeptide 1
AF045464_s_at	1368121_at	Aldo-keto reductase family 7, member A3
K00136mRNA_at	1368180_s_at	LOC494499 protein
AF025670_g_at	1368305_at	Caspase 6
D86745cds_s_at	1368376_at	Nuclear receptor subfamily 0, group B, member 2
U06274_s_at	1368397_at	UDP glycosyltransferase 2 family, polypeptide B4
AF087943_s_at	1368490_at	CD14 antigen
U73174_at	1369061_at	Glutathione reductase
AF068202_at	1369069_at	A kinase (PRKA) anchor protein 1
D13122_f_at	1369588_a_at	ATPase inhibitor
L11007_at	1369950_at	Cyclin-dependent kinase 4
rc_AI233261_i_at	1370030_at	Glutamate cysteine ligase, modifier subunit
rc_AI171506_at	1370067_at	Malic enzyme 1
D16478_at	1370164_at	Hydroxyacyl-Coenzyme A dehydrogenase/3-ketoacyl-Coenzyme A thiolase/enoyl-Coenzyme A hydratase (trifunctional protein), alpha subunit
U33500_g_at	1370566_at	retinol dehydrogenase 2
J05132_s_at	1370613_s_at	UDP glycosyltransferase 1 family, polypeptide A1
J05181_at	1370688_at	Glutamate-cysteine ligase, catalytic subunit
M13506_at	1370698_at	Liver UDP-glucuronosyltransferase, phenobarbital-inducible form
AJ001517cds_at	1370772_a_at	Hemochromatosis
S72506_s_at	1371089_at	Glutathione *S*-transferase Yc2 subunit
M20629_s_at	1371100_at	Esterase 2
M11794cds#2_f_at	1371237_a_at	Metallothionein
S70011_g_at	1372715_at	Sideroflexin 1 (predicted)
S55305_s_at	1386866_at	Tyrosine 3-monooxgenase/tryptophan 5-monooxgenase activation protein, gamma polypeptide
L07736_at	1386946_at	Carnitine palmitoyltransferase 1, liver
X04229cds_s_at	1386985_at	Glutathione *S*-transferase, mu 1
M33329_f_at	1387006_at	Rat senescence marker protein 2A gene, exons 1 and 2
E03424cds_s_at	1387221_at	GTP cyclohydrolase 1
M30282_at	1387323_at	Kallikrein B, plasma 1
M95762_at	1387372_at	Solute carrier family 6, member 13
J02679_s_at	1387599_a_at	NAD(P)H dehydrogenase, quinone 1
M26125_at	1387669_a_at	Epoxide hydrolase 1
X55286_g_at	1387848_at	3-Hydroxy-3-methylglutaryl-Coenzyme A reductase
rc_AI072634_at	1388155_at	Keratin complex 1, acidic, gene 18
D17309_at	1398310_at	Aldo-keto reductase family 1, member D1

Table 5. Continued.

rc_AI012807_at	1398765_at	Adaptor-related protein complex 2, mu 1 subunit
S56936_s_at	none	–
S82820mRNA_s_at	none	–
M33747_at	none	–
rc_AI638982_at	none	–
M33746mRNA#2_f_at	none	–
D00362_s_at	none	–
AF044574_at	none	–
S80431_s_at	none	–
rc_AI236284_s_at	none	–
M29249cds_at	none	–
D86745exon_s_at	none	–
X57133mRNA_at	none	–
X74565cds_g_at	none	–
U05784_s_at	none	–
AF087944mRNA_s_at	none	–
X77934cds_at	none	–
rc_AA859519_g_at	none	–
X57999cds_at	none	–
rc_AI231807_g_at	(1367559_at)	–
K01932_f_at	(1367774_at)	–
S72505_f_at	(1367774_at)	–
D00569_at	(1367777_at)	–
D86580_at	(1368376_at)	–
S65555_g_at	(1370030_at)	–

Probe sets whose signals were reported as increased by treatment of glutathione depletors in RG U34A GeneChip analysis were selected from the previous literature, and the corresponding probe sets of RAE 230A GeneChip were determined by referring to "good match probe sets" information provided by Affymetrix. Eighteen probe sets of RG U34A GeneChip did not show any corresponding probe sets in RAE 230A GeneChip, and were presented as "none" in the table. Six probe sets of RG U34A GeneChip had redundant probe sets for the same genes, and the corresponding probe sets are presented in brackets in the table.

was determined by logarithmic conversion of the fold change, where the base was set to 2. The heat map was created using Spotfire software (Spotfire, Inc.). The CYP1A1 mRNA level was determined by referring to signal data measured by 1370269_at gene probe set in GeneChip analysis.

RESULTS

TGP1 score

The TGP1 scores for carcinogenesis-related genes, PPARα-regulated genes and glutathione deficiency-related genes were calculated. For carcinogenesis-related genes, OPZ, CPZ, HCB, SS and WY showed a high TGP1 score among the compounds in the database (Fig. 2 A). For PPARα-regulated genes, WY, CFB, GFZ, BBr and ASA showed high TGP1 score (Fig. 2 B). For glutathione deficiency-related genes, OPZ, BBz, APAP and CMA showed high TGP1 score (Fig. 2 C).

In order to see the dose-dependency of the score, we selected several samples and showed them in Fig. 3A (carcinogenesis-related genes), 3B (PPARα-regulated genes), and 3C (glutathione deficiency-related genes) . It is obvious that the score showed good dose-dependency for all three of the marker gene sets. It is also interesting that some drugs show a sudden and large rise of the score suggesting a threshold of the toxicity at a certain dose level.

Comparison of TGP1 score between rat liver and rat hepatocytes

The TGP1 scores of rat liver and rat hepatocytes were calculated. For carcinogenesis-related genes, the